Melting and Accumulation Characteristics of Ice Crystals in Aero-engines

CHEN Jiajun[1], *LIU Xiufang*[1,2*], *ZHONG Fuhao*[1], *MIAO Qingshuo*[1], *ZHENG Mian*[1], *WEI Zhen*[1], *HOU Yu*[1]

1. School of Energy and Power Engineering, Xi'an Jiaotong University, Xi'an 710049, P.R.China; 2. Key Laboratory of Icing and Anti/De-icing of China Aerodynamics Research and Development Center(CARDC), Mianyang 621000, P. R. China

(Received 26 March 2023; revised 4 December 2023; accepted 5 December 2023)

Abstract: Ice crystal icing has the potential to induce engine damage or flameout, posing a serious threatening to flight safety. Therefore, it is of great importance to improve the precision of ice crystal icing prediction. Considering the effect of blade thickness, we develop a numerical model to simulate the entire process of ice crystal icing. The influences of airflow parameters, ice crystal suction position and blade thickness are examined on the characteristics of ice crystal melting and accumulation. The findings show a high melting rate of ice crystals at high air velocities, accompanied by a relatively short heat transfer duration, resulting in a low liquid water content. The trajectories of ice crystals at different suction positions are simulated, which reveals that elastic collision occurs at the first two blades, while adhesion takes place at the last three blades. The effect of blade thickness is found to be significant. The ice accumulation area is expanded, the main ice accumulation is shifted toward stators backwards, and the ice accumulation in each stator is more concentrated after taking blade thickness into account.

Key words: ice crystal icing; airflow parameters; melting characteristics; collision behavior; ice accumulation characteristics

CLC number: V231 **Document code:** A **Article ID:** 1005-1120(2023)06-0653-10

0 Introduction

The inhalation of ice crystals into aero-engines can result in a loss of engine power and damage to engine components[1]. The melting and freezing mechanism of ice crystals inhaled by an engine is rather complicated, and its understanding remains elusive[2]. As shown in Fig.1, ice crystals undergo heat and mass exchange with the airflow through melting, and consequently forming ice-water mixture. Afterward, these crystals collide with the engine blade surface, where some of them bounce and break, while others adhere to the surface and form ice accumulation[3]. To accurately predict engine ice accumulation, it is crucial to identify the underlying mechanisms of ice crystal melting and ice accumulation.

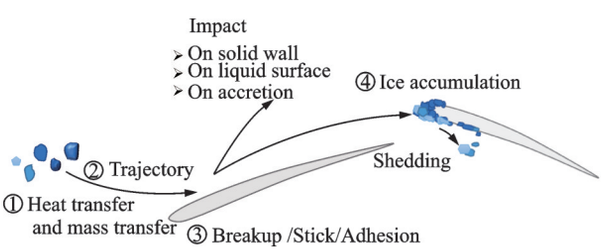

Fig.1 Mechanism of ice crystal accumulation in aero-engines

The melting of ice crystals has been studied in different air flow environments. Han et al.[4] proposed a double-layer ice crystal melting model which considers the effects of ambient temperature, relative humidity and saturated vapor density on ice crystal melting. The model can accurately predict the melting process of ice crystals under natural convection. Yang et al.[5] investigated the melting char-

*Corresponding author, E-mail address: liuxiufang@mail.xjtu.edu.cn.

How to cite this article: CHEN Jiajun, LIU Xiufang, ZHONG Fuhao, et al. Melting and accumulation characteristics of ice crystals in aero-engines[J]. Transactions of Nanjing University of Aeronautics and Astronautics, 2023, 40(6): 653-662.

http://dx.doi.org/10.16356/j.1005-1120.2023.06.003

acteristics of ice crystals in forced convection environment. Recent studies have shown that airflow parameters such as airflow temperature and airflow velocity have great influence on the melting process of ice crystals. Zhang et al.[6] and Zhu et al.[7] simulated the melting process of non-spherical ice crystals under the condition of engine airflow, and obtained the distribution function of liquid water content versus the axial position of ice crystals. Ma et al.[8] also considered the influence of non-spherical factors on ice crystal melting. Bartkus et al.[9] simulated the melting process of ice crystals in a frozen wind tunnel under a thermal flow environment, and found that airflow temperature and humidity have a significant influence on ice crystal melting. Guo et al.[10] claimed that the airflow temperature has direct impact on the wet bulb temperature, and in turn affects the ice crystal melting.

Ice crystals in airflow melt partially and move along. After collision with the wall, three potential outcomes could occur depending on the magnitude of the collision kinetic energy: Breakup, elastic collision and adhesion. Among the three behaviors, adhesion has a major influence on the engine performance. Veres et al.[11] showed that the formation of adhesive ice requires the wet-bulb temperature to be lower than 0 ℃ and a high liquid water content. One experimental study of Tom et al.[12] confirmed that liquid water content is a key factor for the icing of ice crystals. As the liquid water content increases from 5% to 10%, the ice thickness increases significantly. Liu et al.[13] built a measurement platform for shear adhesion, and the experimental results show that an increase of the water temperature promotes nucleation of ice crystals and increases adhesion strength. In addition, there are also efforts made to predict ice accumulation. Norde[14] simulated the entire lifetime of ice crystal including its motion trajectory, melting, collision and adhesion to ice accumulation in the airflow. Shezad et al.[15] established a mixed-phase icing model involving air, water droplets and ice crystals, and applied this model to the icing prediction of NACA0012 airfoil. Jiang et al.[16] developed a model for ice crystal accumulation in turbofan engines. They found that ice crystals with diameter of 20 μm exhibit adhesion, while those of 100 μm do not adhere due to a low liquid water content.

The melting and freezing mechanism of ice crystals ingested by aero-engines is a complex phenomenon which has received limited attention hitherto. Therefore, further investigation is necessary to address the complexity by revealing the underlying mechanisms. Among the few relevant studies, Jiang et al.[16] showed a complete simulation method for ice crystal accumulation in turbofan engine. It forms the basis for the simulation of ice crystal motion, heat transfer, collision adhesion and other behaviors. For simplicity, blade thickness is often ignored although it could affect ice melting and accumulation outcomes. In this study, we numerically investigate the motion, heat transfer, adhesion and ice accumulation induced by ice crystals ingestion into aero-engines by taking blade thickness into consideration. The objectives of this study involves investigating the melting characteristics of ice crystals under varying air flow parameters, analyzing the trajectories and collision behaviors of ice crystals at different initial inhalation positions at the engine inlet port, revealing the height and distribution of ice accumulation under freezing conditions, and comparing the differences in ice accumulation between blades with and without thickness, so as to reveal how blade thickness influences the ice accumulation process.

1 Numerical Model

The numerical model is developed to cover the entire process of ice crystals ingested into the engine, including moving dynamics, behaviors of collision, adhesion and accumulation, and heat transfer and phase change (melting and sublimating) alongside these behaviors in the hot airflow. The numerical model for each process is described as follows.

1.1 Aero-engine flow channel model

Fig.2 illustrates the first five stages of the low-pressure compressor (LPC) of the engine. Each stage is composed of rotors and stators. In Fig.2,

S1 to S5 indicate the five stators, and R1 to R5 the five rotors of LPC. The model is employed to simulate the velocity, temperature and pressure fields as air is flowing through the low-pressure compressor. The flow parameters and geometric parameters are in accordance with those in Refs.[16-17].

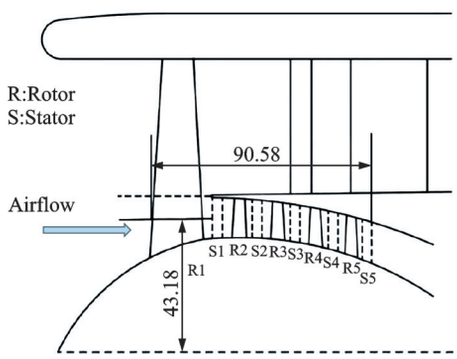

Fig.2 Schematic of the fan and LPC portion of the engine

1.2 Heat and mass transfer model of ice crystal

The entire transition of ice crystals from initial icing condition to water in hot airflow is divided into three stages, as shown in Fig.3. The first stage is sublimation of supercooled ice crystals where the main heat transfer mechanism is convection. The second one is the formation of ice-water mixture where melting develops toward the crystal core while evaporation occurs at the water-gas interface. The third one is the melting and evaporation of ice-water mixture, and at the end it is fully melt to water. This study is focused on the first two stages. The governing equations describing the heat and mass transfer of the ice crystal can be referred to Refs.[14-15].

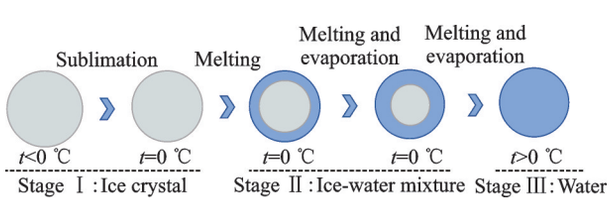

Fig.3 Schematic diagram of ice crystal melting process

Stage Ⅰ

Heat transfer

$$hA(T_{air}-T_{ice})+L_{sg}\frac{dM_{ice}}{dt}=C_{pi}M_{ice}\frac{dT_{ice}}{dt} \quad (1)$$

$$Nu=2+0.55Pr^{\frac{1}{3}}Re^{\frac{1}{2}} \quad (2)$$

$$h=\frac{Nu\cdot\lambda_{air}}{D_i} \quad (3)$$

where h is the convective heat transfer coefficient of ice crystal, A the surface area of ice crystal, T_{air} the temperature of air, T_{ice} the temperature of ice crystal, L_{sg} the latent heat of melting, λ_{air} the thermal conductivity of air, D_i the diameter of ice crystal, M_{ice} the mass of ice crystal and C_{pi} the specific heat capacity of ice crystal.

Mass transfer

$$\frac{dM_{ice}}{dt}=h_mA(\rho_{ga}-\rho_{gi}) \quad (4)$$

$$h_m=\frac{h}{\rho_{air}C_{pa}Le^{2/3}} \quad (5)$$

where h_m is the mass transfer coefficient of ice crystal surface, ρ_{ga} the density of water vapor in air, ρ_{gi} the saturated water vapor density on the ice crystal surface, ρ_{air} the density of air, and C_{pa} the specific heat capacity of air.

Stage Ⅱ

Heat transfer:

$$hA(T_{air}-T_{ice})=L_{lg}\frac{dM_{water}}{dt}+L_{sl}\frac{dM_{ice}}{dt} \quad (6)$$

where L_{lg} is the latent heat of water vaporization, L_{sl} the latent heat of ice crystal melting, and M_{water} the mass of water.

Mass transfer: The water at the surface of the ice-water mixture evaporates and results in a loss of mass

$$\frac{dM_g}{dt}=h_mA(\rho_{gl}-\rho_{ga}) \quad (7)$$

$$M_{mix}=M_{ice}+M_{water}=M_{mix,in}-M_g \quad (8)$$

where ρ_{gl} is the density of saturated water vapor on the surface of the ice-water mixture, ρ_{ga} the density of water vapor, M_{mix} the mass of ice-water mixture, M_g the mass of water vapor that has evaporated, and $M_{mix,in}$ the initial mass of ice-water mixture.

1.3 Motion and collision model of ice crystal

Ice crystal movement is affected by viscous force, pressure differential force and gravity[16]. The density of ice crystals is two-orders of magnitude greater than that of air, resulting in a pressure differential force 1/100 of the viscous force. Since the di-

ameter of ice crystals is about 50 μm, the gravity force is negligible. As a result, only the viscous force is considered in ice crystal motion.

$$\frac{\mathrm{d}\boldsymbol{u}_{\mathrm{ice}}}{\mathrm{d}t}=\frac{3C_{\mathrm{D}}\rho_{\mathrm{air}}}{8\rho_{\mathrm{ice}}R_{\mathrm{ice}}}|\boldsymbol{u}_{\mathrm{air}}-\boldsymbol{u}_{\mathrm{ice}}|(\boldsymbol{u}_{\mathrm{air}}-\boldsymbol{u}_{\mathrm{ice}}) \tag{9}$$

where C_{D} is the drag coefficient of ice crystals, R_{ice} the radius of ice crystal, $\boldsymbol{u}_{\mathrm{air}}$ the velocity of airflow, and $\boldsymbol{u}_{\mathrm{ice}}$ the velocity of ice crystal.

For C_{D}, a relation derived by Clift et al.[18] is applied

$$C_{\mathrm{D}}=\begin{cases}\dfrac{24}{Re}(1+0.15Re^{0.687}) & Re<800\\ 0.28+\dfrac{6}{Re^{0.5}}+\dfrac{21}{Re} & 800<Re<4\,000\end{cases} \tag{10}$$

The geometrical parameters, e.g. thickness, of the compressor blade should be considered. As shown in Fig. 4, the blade is simplified as a two-dimensional planar cascade in this study. The thickness distributions of stators and rotors are based on the NACA airfoil family[19].

$$y=\pm\frac{c}{0.2}(0.296\,90\sqrt{x}-0.126\,00x-0.351\,60x^2+0.284\,30x^3+0.101\,50x^4) \tag{11}$$

where c is the relative thickness ($c=5\%$), and x and y are the dimensionless transverse and vertical coordinates of blade profile relative to chord length, respectively.

According to the NASA experimental data[20], when the liquid water content of ice crystals is above 10%, adhesion will occur. Veres et al.[17] also applied this conclusion to evaluate the risk of ice accretion due to ice crystal ingestion in a turbofan engine. Fig.5 shows the ice crystal collision model. Two behaviors after ice crystals collide with the blades are taken into consideration. Elastic collision occurs when the liquid water content of ice crystals is below 10%, and adhesion occurs otherwise. The velocity $\boldsymbol{U}_2$ after elastic collision is calculated by superposition of two orthogonal velocity vectors.

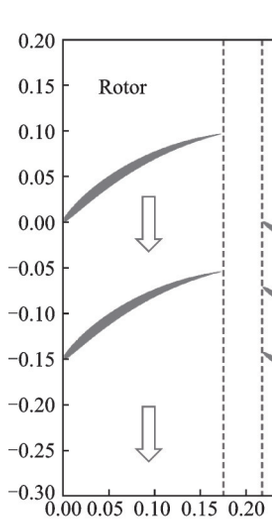

Fig.4 Schematic diagram of rotor and stator blade profiles

Elastic collision

$$\boldsymbol{U}_2=\boldsymbol{U}_{n2}+\boldsymbol{U}_{\tau 2} \tag{12}$$

Adhesion after collision

$$\boldsymbol{U}_2=\boldsymbol{0} \tag{13}$$

where n is the tangential direction of the impact point on the blade surface, and τ the normal direction.

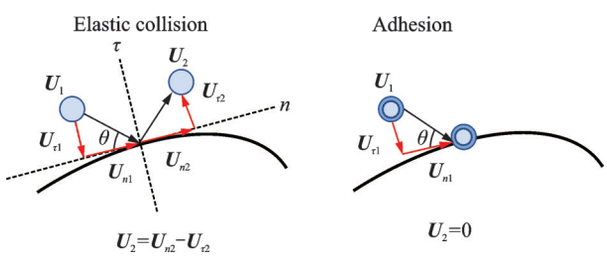

Fig.5 Schematic diagram of ice crystal collision

1.4 Accumulation model of ice crystals

It is assumed that there are 1 000 ice crystals distributed equidistantly in the space between two blades at the entrance of the first-stage rotor. The ice crystal adhesion rate at the blade position can be determined by

$$\varphi(i)=\frac{W(i)N_1/N_2}{1\,000N_1}=\frac{W(i)}{1\,000N_2} \tag{14}$$

where i is the location of ice crystals, $\varphi(i)$ the ice crystal adhesion rate at position i, $W(i)$ the number of ice crystals at position i, N_1 the number of blades of fan, and N_2 the number of blades of stator.

In turn, the ice accumulation height at each position of the blade can be calculated, and the shape of ice of each stage could be obtained.

$$h(i)=\frac{V\cdot\mathrm{IWC}\cdot\varphi(i)}{\rho_{\mathrm{ice}}\cdot\Delta H_{\mathrm{in}}\cdot\Delta C} \tag{15}$$

where $h(i)$ is the ice thickness at position i, V the volume flow at the entrance, IWC the ice content in

the air, $\triangle H_{in}$ the radial length at the entrance, and $\triangle C$ the length of stator blades.

1.5 Solution process

The forward difference method is used to solve the equations. The equations are discretized in time with the time step $dt=10^{-7}$ s to make sure that the courant number is less than 1. First, the parameters of a single ice crystal at time $t+dt$ are computed. The physical properties of ice crystals are obtained by solving Eqs.(1, 4, 6, 7, 9). Afterward, the ice crystal parameters are iterated to initiate the next time step until the completion of ice crystal motion. After the simulation of movement of all ice crystals, the ice shape is determined by solving Eqs.(14, 15).

1.6 Model validation

In order to verify the accuracy of the proposed model. The motion and heat transfer of ice crystals under different airflow conditions with an initial radius of 20 μm and an initial temperature of −20 ℃ is calculated. Fig.6 compares the simulation results of this paper with those of Jiang et al.[16]. The results show that the proposed model has little deviation from Ref.[16]. Therefore, the proposed model can be simulated in the next step.

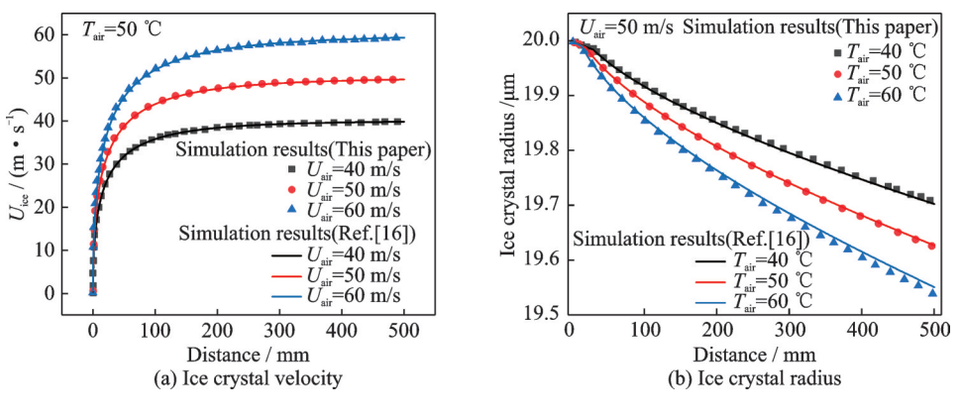

Fig.6 Comparison of numerical simulation results of ice crystal motion and heat transfer with results of Ref.[16]

2 Result Analysis

2.1 Effect of airflow parameters on ice crystal melting

The airflow parameters used in this simulation refer to the airflow conditions inside the low-pressure compressor. The flow rate ranges from 30 m/s to 100 m/s, and the air temperature ranges from 30 ℃ to 65 ℃. The relative humidity is 10%. The initial diameter of ice crystal is 20 μm, and the initial temperature is −20 ℃.

As shown in Fig.7(a), the ice crystal velocity increases rapidly at first and then it approaches the air velocity. Figs.7(b) and (c) show that at a lower air velocity, the radius of ice crystals is smaller and the liquid water content is higher. However, it is found in Fig.7(d) that the higher the air velocity, the higher the melting rate. This is because although a high airflow velocity facilitates the heat and mass transfer of ice crystals, the time of ice crystals staying in the airflow is rather short. As a result, the liquid water content is lower.

Figs.8(a) and (b) show that the higher the air temperature, the smaller the ice crystal radius, and the higher the liquid water content. Specifically, when the air temperature is 35 ℃, the liquid water content is 30%. When the air temperature is 65 ℃, the liquid water content is 99%, and the ice crystals would completely melt into water. In addition, it can be seen from Fig.8(c) that the higher the air temperature, the earlier the ice crystals transit from supercooled state to the ice-water mixture. Therefore, the air temperature has a great influence on ice crystal melting. This effect is greater than that of air velocity, since the larger temperature difference facilitates the heat and mass transfer of the ice crystals.

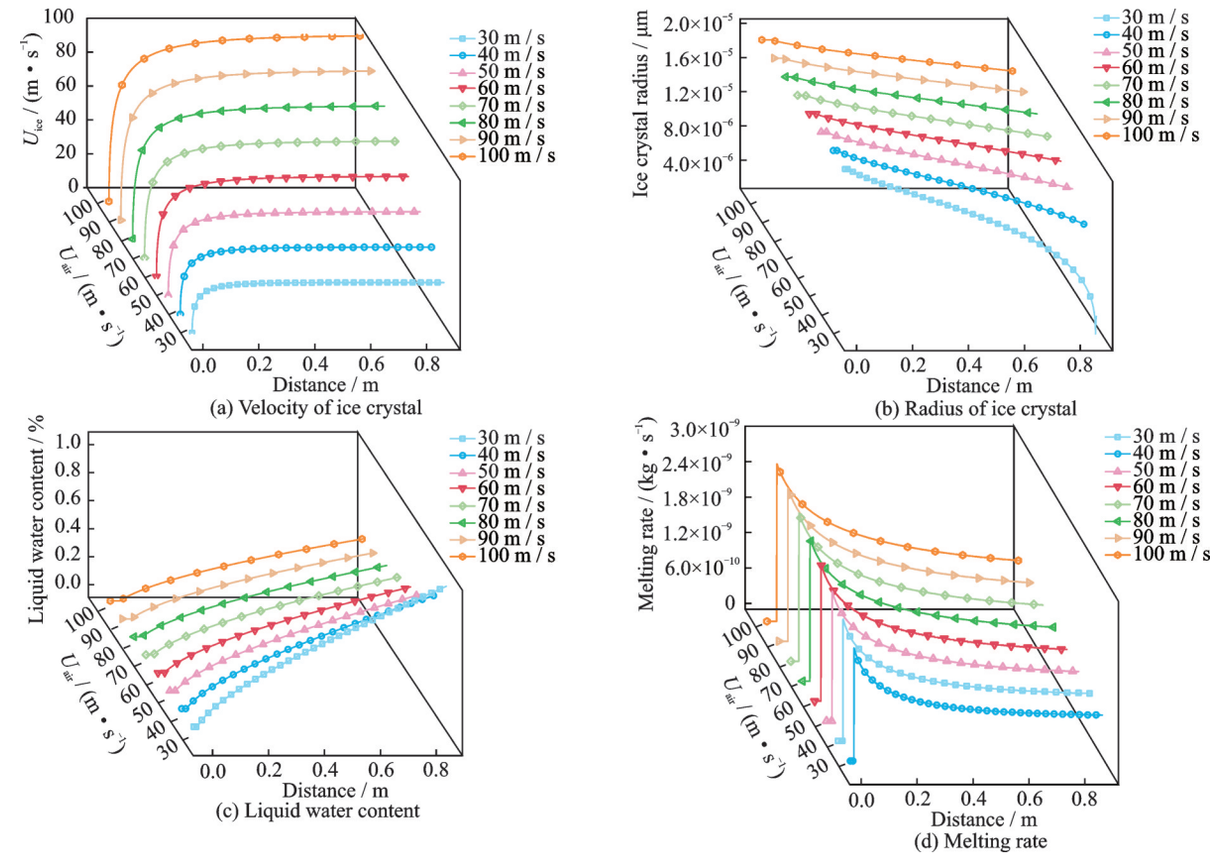

Fig.7 Influence of airflow velocity on ice crystal melting

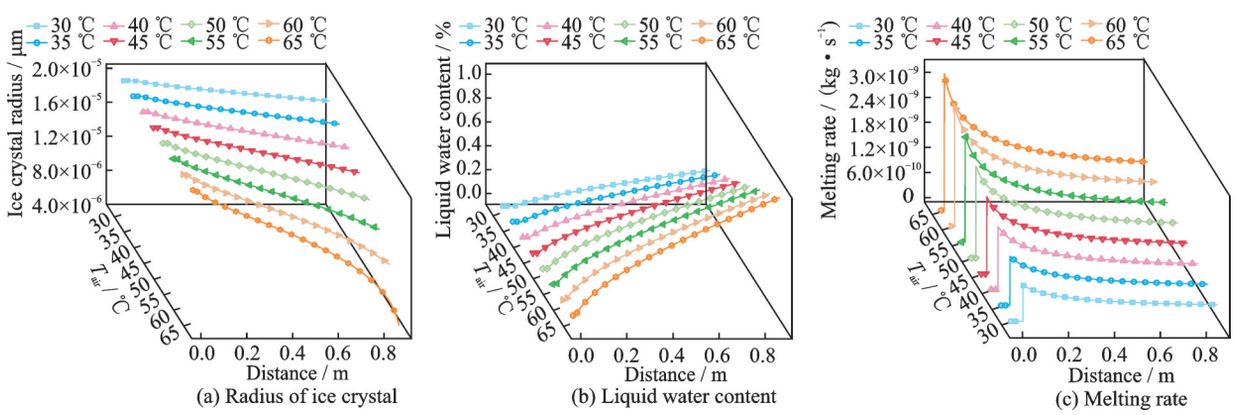

Fig.8 Influence of airflow temperature on ice crystal melting

2.2 Motion trajectories and collision behavior of ice crystals in aero-engine

Fig.9 shows that the liquid water content remains almost constant along the axial direction at the first stage rotors and stators. The liquid water content in the third stage rotors is above 10%, indicating a risk of ice accumulation.

When the ice crystals are ingested into the engine, they gradually melt in hot air. When the liquid water content is below 10% or ice crystals collide with the rotors, elastic collision ensues (shown in brown circle). When the liquid water content is higher than 10% and ice crystals collide with stators, ice crystals adhere to the surface (shown in purple circle).

Fig.9 also shows that there are great differences in the movements of ice crystals at different initial inhalation positions at the engine inlet port. At the 20% position (gray tracks), the ice crystal experiences a sequence of elastic collision with R1, S1, S2, R4. Finally, the ice crystal liquid water content is 37.5% when it collides with S4, resulting in adhesion. At

the 40% position (red trace), the ice crystal undergoes elastic collision with R1 and S2 in sequence, and adheres to S4 eventually. The ice crystals at the 60% and 80% positions all end up adhering to S3.

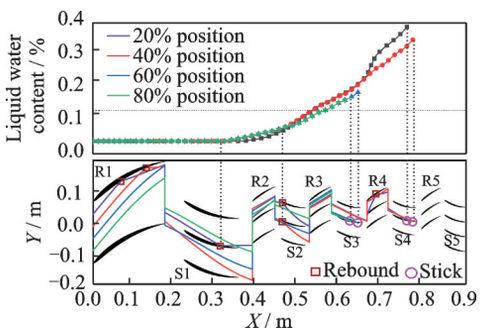

Fig.9 Motion trajectories and liquid water content distribution of ice crystals at different initial positions

2.3 Accumulation characteristics of ice crystal

The adhesion rate of the suction surface and pressure surface of the stators are obtained from the simulation for 1 000 equidistant ice crystals introduced from the entrance. Fig.10 shows that in regardless of the injection location of ice crystals, ice accumulation occurs only on the 3rd, 4th and 5th orders of suction surface, as well as the 2nd, 3rd, 4th and 5th orders of pressure surface of stators.

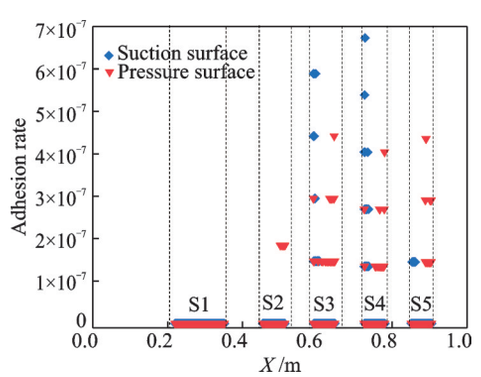

Fig.10 Adhesion rate of ice crystals versus the axial direction X of LPC

Based on the distribution of adhesion rate, the 10 min flight in the cloud with an ice content of 1.5 g/m^3 is simulated, and the accumulated ice profiles on the surface of the stators are shown in Fig.11. It can be seen that S2 has a minor accumulation of ice, while S3, S4 and S5 have significant ice accumulation on the surface.

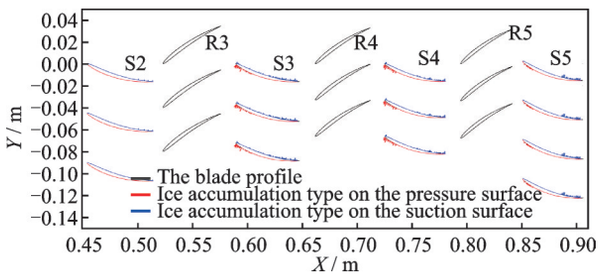

Fig.11 Accumulated ice thickness Y on stators versus the axial position X

Fig.12(a) summarizes the height of ice accumulation on stators. The ice accumulation on the pressure surface is concentrated in the 50% area at trailing edge of the blade. Additionally, the ice accumulation at the 3rd, 4th and 5th stages on the pressure surface is particularly severe, with an average thickness of 1 mm and a maximum thickness of 3 mm. Fig.12(b) shows that the ice accumulation on the suction surface is distributed mainly in 30% of the leading edge of the blade. Compared to the pressure surface, the ice distribution here is more concentrated. The accumulated ice is thicker, reaching a maximum thickness of 2 mm. Specifically, on the 4th stage stator blade, the ice accumulation reaches a maximum thickness of 4 mm.

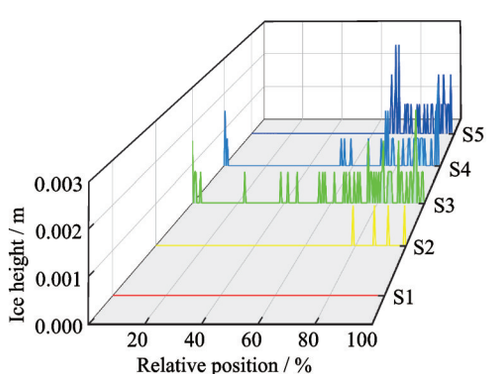

(a) Height of ice accumulation on the pressure surface

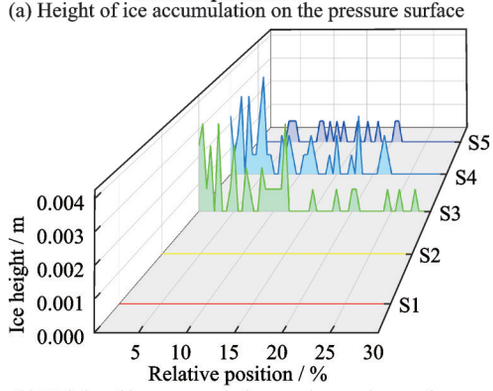

(b) Height of ice accumulation on the suction surface

Fig.12 Height of ice accumulation on stators

The ice accumulation on the stators is a result of the airflow within the stator blades. The airflow direction is dependent on the blade profile. When ice crystals enter the stators, they are more likely to collide with the leading edge of the suction surface. When ice crystals exit the stators, the air flows along the axial direction, driving the ice crystals to collide with the trailing edge of the pressure surface.

Fig.13 shows the difference in ice accumulation on blades with and without thickness. Taking blade thickness into consideration changes the trajectories and collision positions of the ice crystals. In respect to the range of ice accumulation, the blade without thickness (on S2) shows no ice accumulation, whereas a small amount accumulates at the trailing edge of the blade with a thickness. Regarding the main location of ice accumulation, the blade without thickness experiences concentrated ice accumulation S3, whereas the blades with thickness exhibit great accumulation on S3 and S4. For the shape of ice accumulation, the blade without thickness shows a more dispersed pattern, whereas the blade with thickness shows more concentrated ice accumulation at the leading edge.

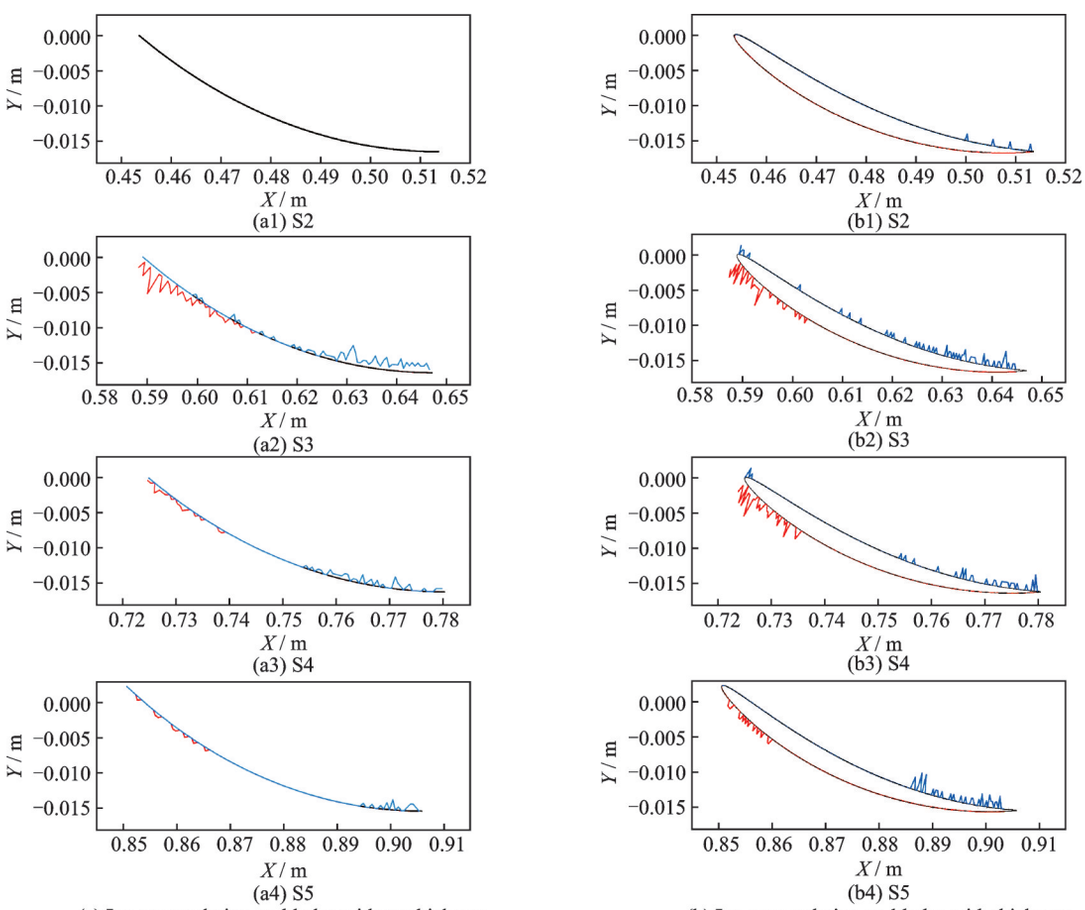

Fig.13 Comparison of ice accumulation on blades without thickness and ones with thickness

3 Conclusions

The entire process of ice crystal accumulation in aero-engine is numerically simulated. The effects of airflow parameters, ice crystal suction position and blade thickness on ice crystal motion, melting and accumulation are investigated. The major findings are summarized as follows.

(1) The melting process of ice crystals is greatly affected by airflow parameters. At a high airflow velocity, the heat and mass transfer time between ice crystals and air is short. Although it results in a higher melting rate, the liquid water content is lower. The temperature of the air flow determines the melting process of ice crystals, and large tempera-

ture differences facilitate notable heat and mass transfer. Therefore, the accurate measurement of the airflow temperature is essential to predict ice crystal icing accurately.

(2) The movement trajectories of ice crystals in the airflow varying significantly is depending on their different initial positions. Elastic collision or adhesion occurs when ice crystals collide with surfaces. The distribution of liquid water content along the axial direction plays a role in determining the type of collision. Elastic collision usually occurs when ice crystals pass through the blades of the first two stages, while adhesion emerges mainly at the blades of the last three stages.

(3) The findings of ice crystal accumulation under the icing condition show that ice accumulation on the pressure surface of the stators is concentrated at 50% of the trailing edge. The average thickness of the ice accumulation is 1 mm, with the maximum thickness of 3 mm. The ice accumulation on the suction surface is concentrated at 30% of the leading edge, which is more pronounced compared to the pressure surface. The average thickness of ice accumulation is 2 mm, with the maximum thickness of 4 mm. Furthermore, the blade thickness significantly affects the range, height and shape of ice accumulation. Including the blade thickness is crucial for accurately predicting and assessing ice accumulation under real operating conditions.

References

[1] SHEN Hao, HAN Bingbing, ZHANG Lifen. Research progress of the ice crystal icing in aero-engines[J]. Journal of Experiments in Fluid Mechanics, 2020,34(6): 1-7.(in Chinese)

[2] HUANG Ping, BU Xueqin, LIU Yiming, et al. Review of icing under mixed phase/ice crystal conditions[J]. Acta Aeronautice et Astronautica Sinica, 2022, 43(5): 120-138.(in Chinese)

[3] YUAN Qinghao, FAN Jiang, BAI Guangchen. Review of ice crystal icing in aero-engines[J]. Journal of Propulsion Technology, 2018, 39(12): 2641-2650.(in Chinese)

[4] HAN Y, KALA S, YAN S, et al. Partial melting time model verification of a levitated ice particle[J]. Cold Regions Science and Technology, 2020, 173: 103013.

[5] YANG X, MCGILVRAY M, GILLESPIE D. Numerical modeling and parametric study of the melting behavior of ice crystal particles[J]. AIAA Journal, 2021, 59(11): 4660-4668.

[6] ZHANG J, CHEN W, ZHANG L. Three-dimensional numerical simulation of ice crystal melting under different influencing factors[J]. Journal of Physics: Conference Series, 2018, 1064: 012026.

[7] ZHU P, ZHANG J, HAN B, et al. Three-dimensional numerical simulation of ice crystal melting in jet engine[J]. Journal of Thermal Science, 2019, 28(5): 984-992.

[8] MA Yijian, CHAI Delin, WANG Qiang, et al. Phase change and adhesion characteristics of ice crystal movements in wing icing[J]. Acta Aeronautice et Astronautica Sinica, 2023, 44(1): 41-52.(in Chinese)

[9] BARTKUS T P, STRUK P, TSAO J C. Development of a coupled air and particle thermal model for engine icing test facilities[J]. SAE International Journal of Aerospace, 2015, 8(1): 15-32.

[10] GUO Qilei, NIU Junjie, AN Bo, et al. Numerical simulation of ice crystal icing under mixed-phase conditions[J]. Acta Aerodynamica Sinica, 2021, 39(2): 168-175.(in Chinese)

[11] VERES J P, JORGENSON P C. Modeling commercial turbofan engine icing risk with ice crystal ingestion[C]//Proceedings of the 5th AIAA Atmospheric and Space Environments Conference. [S.l.]: AIAA, 2013: 2679.

[12] TOM C, DAN F. Experimental results for ice crystal icing on hemispherical and double wedge geometries at varying mach numbers and wet bulb temperatures: AIAA-2016-3740[R]. Reston, VA: AIAA, 2016: 53-98.

[13] LIU Zhenguo, WANG Yusong, ZHU Chengxiang, et al. Effect of water temperature on ice adhesion strength based on nucleation theory[J]. Advances in Aeronautical Science and Engineering, 2022, 13(2): 64-70.(in Chinese)

[14] NORDE E. Eulerian method for ice crystal icing in turbofan engines[M]. Enschede: Ipskamp Printing, 2017.

[15] SHEZAD N, WAGDI G H. Multiphase approach toward simulating ice crystal ingestion: AIAA-2011-2514[R]. Reston, VA: AIAA, 2011: 59-74.

[16] JIANG Feifei, DONG Wei, ZHENG Mei, et al. Phase change heat transfer characteristic of ice crystal ingested into turbofan engine[J]. Journal of Aerospace Power, 2019, 34(3): 567-575.(in Chinese)

[17] VERES J, JORGENSON P, WRIGHT W. A model to assess the risk of ice accretion due to ice crystal in-

gestion in a turbofan engine and its effects on performance[C]//Proceedings of the 4th AIAA Atmospheric and Space Environments Conference. [S.l.]: AIAA, 2012.

[18] CLIFT R, GRACE J R, WEBER M E. Bubbles, drops, and particles[M]. [S.l.]: Academic Press, 1978: 111-112.

[19] FEULNER M, LIAO S, ROSE B, et al. Ice crystal ingestion in a turbofan engine[C]//Proceedings of SAE International Conference on Icing of Aircraft. [S.l.]: SAE, 2015.

[20] STRUK P, CURRIE T, WRIGHT W B, et al. Fundamental ice crystal accretion physics studies[C]//Proceedings of SAE 2011 International Conference on Aircraft and Engine Icing and Ground Deicing. [S.l.]: SAE, 2011.

Acknowledgements This study is supported by the Key Laboratory of Icing and Anti/de-icing of CARDC (No. IADL 20220107), the National Science and Technology Major Special Funds of China (No.J2019-Ⅲ-0010-0054), and the National Natural Science Foundation of China (No. 52076164).

Authors Mr. **CHEN Jiajun** received the B.S. degree in energy and power engineering from Xi'an Jiaotong University in 2021. His research interests include refrigeration and cryogenic technology in aerospace.

Dr. **LIU Xiufang** received the Ph.D. degree in power engineering and engineering thermophysics from Xi'an Jiaotong University in 2013. She is currently an associate professor in School of Energy and Power Engineering, Xi'an Jiaotong University, Shaanxi, China. Her research interests include refrigeration and cryogenic technology in aerospace, thermal management technology and cryogenic multi-phase flow, etc.

Author contributions Dr. **LIU Xiufang** designed the study and conducted the analysis. Prof. **HOU Yu** provided suggestions for the theoretical part and structure of the manuscript. Mr. **CHEN Jiajun** interpreted the results and wrote the manuscript. Mr. **ZHONG Fuhao** contributed to data for the analysis of the manuscript. Mr. **MIAO Qingshuo**, Ms. **ZHENG Mian** and Mr. **WEI Zhen** contributed to the discussion and background of the study. All authors commented on the manuscript draft and approved the submission.

Competing interests The authors declare no competing interests.

(Production Editor: WANG Jing)

航空发动机内冰晶的融化特性和积冰特性

陈佳军[1], 刘秀芳[1,2], 钟富豪[1], 苗庆硕[1], 郑 勉[1], 魏 震[1], 侯 予[1]

(1.西安交通大学能源与动力工程学院,西安 710049,中国; 2.中国空气动力研究与发展中心结冰与防除冰重点实验室,绵阳 621000,中国)

摘要:冰晶结冰可能导致发动机损坏或熄火,严重威胁飞行安全,因此提高冰晶结冰预测的精度意义重大。本文考虑叶片厚度的影响,建立了冰晶结冰全过程的数值模型,探究了气流参数、冰晶吸入位置和叶片厚度对冰晶融化特性和积冰特性的影响。研究结果表明,在高风速下,冰晶的融化速度快,传热时间短,导致液态水含量低。不同吸入位置的冰晶在内流道的运动轨迹表明,冰晶在前两级叶片发生弹性碰撞,而在后三级叶片发生粘附。叶片厚度对冰晶结冰特性的影响显著,考虑叶片厚度后,积冰面积扩大,主积冰区域沿定子叶片尾缘后移,各定子叶片积冰更加集中。

关键词:冰晶结冰;气流参数;融化特性;碰撞行为;积冰特性